Ninth International Conference on CFD in the Minerals and Process Industries
CSIRO, Melbourne, Australia
10-12 December 2012

MULTI-SCALE VOLUME OF FLUID MODELLING OF DROPLET COALESCENCE

Lachlan R. MASON, Geoffrey W. STEVENS and Dalton J. E. HARVIE*

Department of Chemical and Biomolecular Engineering, The University of Melbourne, Victoria 3010, AUSTRALIA
*Corresponding author, E-mail address: daltonh@unimelb.edu.au

ABSTRACT

Coalescence behaviour in liquid–gas systems influences droplet size and velocity distributions, affecting macro-scale heat and mass transfer characteristics. Quantifying the regimes in which coalescence occurs is therefore important for the design and optimisation of engineering applications including fuel injection, spray cooling and spray drying.

We use a multi-scale simulation method to investigate the coalescence behaviour of liquid droplets undergoing a symmetric binary collision. A subgrid-scale model is included to account for thin-film drainage due to the computational difficulty of capturing all length scales involved with a single discretisation mesh. Fluid dynamics within the droplets is modelled using a coupled volume of fluid (VOF) code.

Modelling of collision events is validated through comparison with experimental collisions reported in the literature for tetradecane droplets in air. The present results will aid in the future improvement of simulation techniques for coalescence processes.

NOMENCLATURE

a	regression constant
F	volume-fraction colour function
$\mathbf{f}_\mathrm{b}$	surface volume force, N/m^3
$\mathbf{g}$	gravitational acceleration, m/s^2
H	dimensionless interface region width
h	gas-film thickness, m
$\hat{\mathbf{n}}$	unit normal vector
p	pressure, Pa
R	droplet radius, m
$\mathbf{r}$	position vector, m
r	radial coordinate, m
t	time, s
t_m	elapsed simulation time, s
U	parasitic velocity current, m/s
$\mathbf{u}$	liquid velocity, m/s
u_r	liquid radial velocity, m/s
u_z	liquid axial velocity, m/s
v_r	gas-film radial velocity, m/s
v_z	gas-film axial velocity, m/s
W	dimensionless interface region width ($W = w/\Delta x$)
w	interface region width, m
We	Weber number ($We = \rho d u_{\mathrm{rel},0}^2/\sigma$)
Δx	cell width, m
z	axial coordinate, m

Greek letters

κ	curvature, 1/m
μ	dynamic viscosity, Pa s
ρ	density, kg/m^3
σ	surface tension, N/m

Subscripts

0	initial
A	advection
crit	critical
film	gas thin film
g	gas
l	liquid
max	maximum
P	parasitic
r	radial component
rel	relative
T	transient
V	viscous
z	axial component

INTRODUCTION

Collisional behaviour of liquid droplets is important in many process engineering applications including spray cooling (Jia and Qiu, 2003), coating (Mostaghimi *et al.*, 2003) and liquid fuel combustion (Ashgriz and Givi, 1989). Coalescence or bouncing collision outcomes can influence macro-scale system characteristics including heat and mass transfer rates. Hence, a detailed understanding of the coalescence process is important for the design and optimisation of industrial unit operations.

Coalescence is governed by the drainage of the thin gas film separating two colliding droplets. The droplets will bounce if the film does not drain sufficiently during the impact event. Film rupture and subsequent coalescence tends to occur when the film thins to a critical film thickness on the order of 10–50 nm (MacKay and Mason, 1963; Bradley and Stow, 1978). At this length scale, van der Waals surface forces become dominant and film rupture occurs.

Coalescence behaviour has been investigated experimentally using binary droplet collisions (Ashgriz and Poo, 1990; Jiang *et al.*, 1992; Qian and Law, 1997; Rabe *et al.*, 2010). Collision outcomes have been classified depending on the Weber number ($We = \rho d u_{\mathrm{rel},0}^2/\sigma$) into the regimes of (i) coalescence after minor deformation, (ii) bouncing, (iii) coalescence after major deformation, and (iv) separation.

Coalescence has been simulated using a variety of modelling techniques (Janssen and Anderson, 2011) including front tracking (marker-and-cell, boundary integral, immersed boundary) and front capturing (level set, volume of fluid (VOF), lattice Boltzmann, smoothed-particle hydrodynamics, phase field techniques). Front tracking methods have difficulty simulating the entire transition from initial contact to final merging (Cristini and Tan, 2004). Front capturing methods, in contrast, are well suited for modelling the entire process.

Nobari *et al.* (1996) used a front tracking algorithm to model axisymmetric binary collisions. Coalescence was simulated numerically by removing the thin film at a

prescribed time. The evolution of the droplet shape was found to depend on the time chosen. Pan *et al.* (2008) used the same method to investigate the transition between bouncing and coalescence regimes with increasing Weber number. Experimentally determined values of the critical film rupture time (for tetradecane droplets in 1 atm air) were used to determine the time of film removal.

Jiang and James (2007) used a front capturing VOF algorithm to simulate binary collisions of liquid droplets driven by a hyperbolic gas flow. The collision outcome was prescribed by setting the volume-fraction boundary condition using a row of 'ghost cells' on the collision plane: a zero volume fraction represents a completely non-wetting interface and hence will result in bouncing; whereas a symmetry condition represents a wetting interface and hence usually results in coalescence. Li and Fritsching (2011) used a VOF algorithm to simulate the coalescence of tetradecane droplets in nitrogen. Film rupture was modelled by switching the ghost-cell boundary condition (from a zero- to symmetry condition) at a predetermined time.

Nikolopolous *et al.* (2009) used an adaptive-mesh VOF algorithm to simulate symmetric binary collisions. Two volume-fraction colour functions were used to represent each drop up until a prescribed time of film rupture. After this time, coalescence was modelled by combining the two colour functions with a single function.

Multi-scale modelling techniques are amenable to the present system as the film thickness can be four orders of magnitude smaller than the droplet radius. In order to resolve the thin-film dynamics, standard VOF simulations would require use of a high mesh resolution (with a small computational time step and high associated compute time). Multi-scale methods can instead capture the thin-film dynamics with a semi-analytical model, which is coupled to the droplet-scale model. Coupling of film-drainage models to separate macro-scale models has been demonstrated in the literature. Harvie (1999)—see also Harvie and Fletcher (2001)—used a one-dimensional subgrid-scale algorithm to model the viscous vapour layer in a droplet–hot plate collision. Macro-scale droplet evolution was simulated using a VOF method. Thomas *et al.* (2010) used a coupled front-tracking method and subgrid-scale analytical model to simulate the thin film between a liquid droplet and a solid inclined plane. Results obtained using a fine mesh could be recovered using the course-mesh multi-scale method developed. Additional examples of multi-scale models include the coupling of thin-film drainage to a boundary integral model (Davis *et al.*, 1989) and the coupling of gas rarefaction dynamics to a droplet-scale energy balance (Zhang and Law, 2011). Hardt (2005) demonstrated the coupling of electric double layer interaction potentials to a VOF model in a liquid–liquid system.

In this study, we use a coupled VOF and subgrid-scale film-drainage model in order to determine the film rupture time in a physically meaningful way. As this method does not rely on *a priori* empirical determination of the rupture time, it is predictive in nature.

MODEL DESCRIPTION

Volume of fluid model

The present model is based on that of Harvie (1999). The VOF method (Hirt and Nichols, 1981) used makes use of an averaged-volume-fraction colour function F that is advected by the flow:

$$\frac{\partial F}{\partial t} + \mathbf{u}\cdot\nabla F = 0 \tag{1}$$

where:

$$F(\mathbf{r},t) = \begin{cases} 1, & \text{for } \mathbf{r} \text{ in liquid phase} \\ 0, & \text{for } \mathbf{r} \text{ in gas phase} \\ 0 < F < 1, & \text{in the interface region} \end{cases} \tag{2}$$

In this study, effects of the macro-scale gas flow are neglected, meaning that fluid properties are smoothed across the interface using the averaging equations:

$$\rho = F\rho_\mathrm{l} \tag{3}$$

$$\mu = F\mu_\mathrm{l} \tag{4}$$

The velocity field is then determined (for the liquid phase only) using the Navier–Stokes equation:

$$\rho\left(\frac{\partial \mathbf{u}}{\partial t} + \mathbf{u}\cdot\nabla\mathbf{u}\right) = -\nabla p + \mu\nabla^2\mathbf{u} + \mathbf{f}_\mathrm{b} \tag{5}$$

Interfacial forces are included using a surface volume force term $\mathbf{f}_\mathrm{b}$ via the relation

$$\mathbf{f}_\mathrm{b} = \sigma\kappa\nabla F + p_\mathrm{film}\hat{\mathbf{n}}, \tag{6}$$

where σ is the surface tension, κ is the local interfacial curvature and p_film is the cell-averaged local film pressure. As the macro-scale gas flow is neglected, the force term $\mathbf{f}_\mathrm{b}$ is fluid-side weighted (Brackbill *et al.* 1992).

Subgrid-scale gas-film model

The original subgrid-scale model has been previously detailed in Harvie and Fletcher (2001) for droplet–solid collisions. Briefly, for droplets that are close together it is assumed that the film thickness (i) is small compared to the droplet radius, (ii) changes slowly in the radial direction, and (iii) changes at a velocity lower the local gas velocity. These assumptions allow the incompressible Navier–Stokes equations (in cylindrical coordinates) to be reduced to:

$$-\frac{1}{\rho_\mathrm{g}}\frac{\partial p_\mathrm{film}}{\partial z} = 0 \tag{7}$$

$$\frac{\partial^2 v_r}{\partial z^2}(r,z) = \frac{1}{\mu_\mathrm{g}}\frac{\mathrm{d}}{\mathrm{d}r}\left[p_\mathrm{film}(r)\right] \tag{8}$$

Here, v_r is the radial gas velocity. Eqs. (7) and (8) are solved at each time step. The determined local film pressure p_film is then applied to the macro-scale VOF code via the surface volume force $\mathbf{f}_\mathrm{b}$ (Eq. (6) above). An iterative solution method is used to solve Eqs. (1)–(6) and Eqs. (7)–(8) via $p_\mathrm{film}(r)$ and $h(r)$. An outline of the multi-scale modelling approach is shown in Fig. 1.

In order to model a droplet–droplet collision, differing from Harvie (1999), the gas-film radial velocity v_r is assumed to be symmetric over the $z = 0$ collisional plane:

$$\frac{\partial v_r}{\partial z}(r,0) = 0 \tag{9}$$

The same radial velocity is set equal to the local droplet radial velocity u_l at the interface:

$$v_r(r,h/2) = u_\mathrm{l}(r) \tag{10}$$

The gas film is modelled until the critical thickness is reached—we then allow coalescence to occur. Numerically, this is achieved by enforcing either a zero-volume-fraction or symmetric boundary condition in a row of ghost cells on the collision plane. Prior to the film rupture condition the liquid droplets are subject to a zero-

volume-fraction boundary condition, ensuring that coalescence cannot occur. The boundary condition is then switched to the symmetric case for all times following the rupture condition.

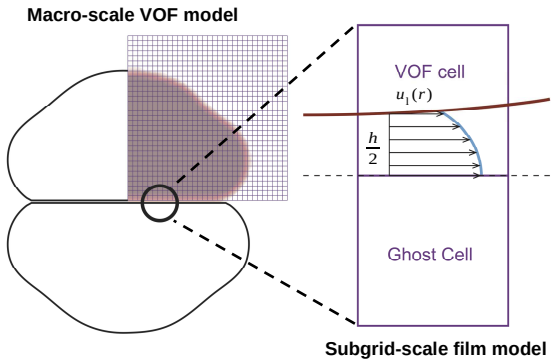

Figure 1: Outline of multi-scale methodology. Two planes of symmetry are assumed in the macro-scale model. The subgrid-scale model and location of ghost cells are also shown

Case-specific details

The experimental symmetric binary droplet collision of Pan *et al.* (2008) is simulated using the parameter values shown in Table 1. Eqs. (1) and (5) are solved using an implicit iterative technique on a two-dimensional staggered mesh of dimensions 60×90. Two planes of symmetry are assumed in VOF model as shown in Fig. 1.

Parameter	Value
μ_l	2.13×10^{-3} Pas
ρ_l	755 kg/m^3
R	170 μm
$u_{rel,0}$	1.19 m/s
σ	0.0267 N/m
We	13.6

Table 2: Simulation parameters corresponding to the experimental collision of Pan *et al.* (2008)

RESULTS

The resultant collision sequence, corresponding to the experimental images of Pan *et al.* (2008), is shown in Fig. 2. Here, the critical film thickness was set to 40 nm and the simulation time scale was uniformly translated to match that of the original experiment. The simulated film ruptures prior to maximum deformation of the droplet as per the experiment ($t = 0.366$ ms in Fig. 2). The evolution of the macro-scale droplet shape also agrees well with the experimental image sequence. Simulation results show the cross section of the droplet shape, meaning that some discrepancies occur (notably at $t = 0.450$ ms and 0.500 ms) as only the silhouette was imaged in the experimental sequence (Pan *et al.*, 2008).

Film-thickness and pressure profiles

Fig. 3 shows the film-thickness time series at (i) the centre of the droplet and (ii) at the radial location observed to first reach the critical rupture thickness. A 'rim rupture' coalescence event occurs as shown by the radial film-thickness profiles in Fig. 4.

Radial gauge pressure profiles for the gas film are shown in Fig. 5. For intermediate time values, a region of negative gauge pressure is observed consistent with the simulation results of Li and Fritsching (2011). For times close to the rupture event, a spike in pressure is observed at the corresponding radial distance of the minimum film thickness ($r = 140$ μm).

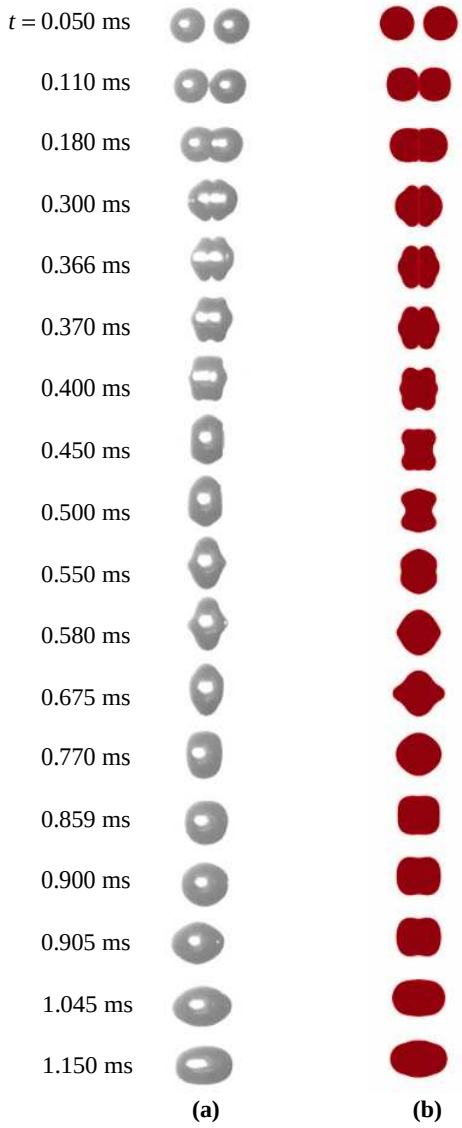

Figure 2: Collision sequence of (a) Pan *et al.* (2008) experiment and (b) present model using $h_{crit} = 40$ nm. Tetradecane droplets in 1 atm air, $R = 170$ μm, $u_{rel,0} = 1.19$ m/s, $We = 13.63$. Reprinted with permission from Pan K.-L., Law, C. K. and Zhou, B., 2008, Experimental and mechanistic description of merging and bouncing in head-on binary droplet collision, *J. Appl. Phys.*, 103, 064901. Copyright 1998, American Institute of Physics.

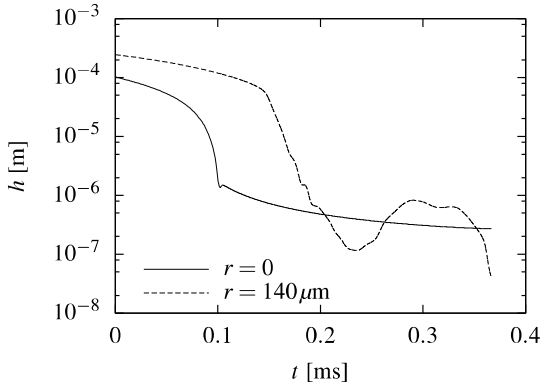

Figure 3: Film thickness time series for the locations $r = 0$ and $r = 140\,\mu m$. The thickness for film rupture was set to $h_{crit} = 40$ nm

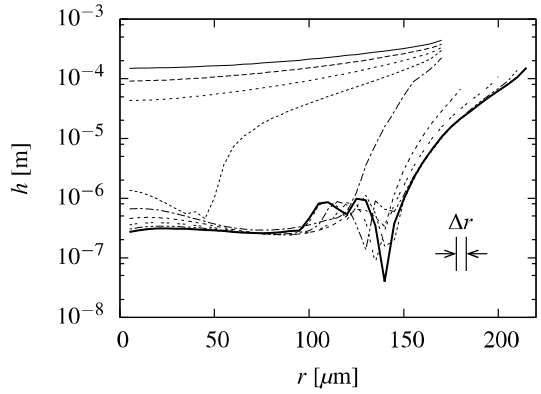

Figure 4: Film thickness (h) profiles at 0.05 ms time intervals. The profile immediately preceding coalescence is shown in bold. The cell width Δr is shown for reference

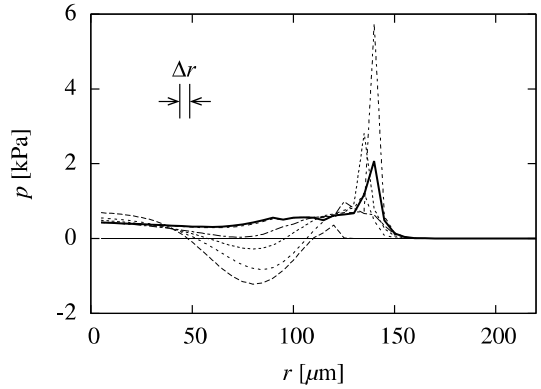

Figure 5: Film gauge pressure profiles at 0.05 ms time intervals. The profile immediately preceding coalescence is shown in bold. The cell width Δr is shown for reference

Rupture time sensitivity

The simulation rupture time $t_{rupture}$ was defined (using the experimental time scale basis) as the first time at which the minimum film thickness was lower than the imposed critical rupture thickness $h_{crit.}$. Note that the actual duration of film drainage will be lower than $t_{rupture}$ as, in this case, the droplets have an initial separation. Fig. 6 shows the sensitivity of $t_{rupture}$ to the imposed value of h_{crit}. The rupture time is shown to increase with decreasing values of h_{crit}, with a sharp increase in sensitivity when h_{crit} is set to be less than 50 nm.

To investigate the sensitivity of the macro-scale droplet evolution to the rupture time, a rupture time $t_{rupture}$ was imposed (rather than predicted via a critical rupture height h_{crit}). The full collision sequence for a series of imposed rupture times (0.2 ms, 0.3 ms, 0.4 ms) is shown in Fig. 7. Immediately prior to film rupture, the macro-scale droplet shape was found to be dependent on the rupture time imposed. For the lowest critical rupture time of 0.2 ms (Fig. 7a), rupture is observed to occur before the maximum deformation of the droplet. For the highest critical rupture time of 0.4 ms (Fig. 7c), coalescence occurs after the maximum droplet deformation. Despite these marked differences, the evolution of the droplet shape at large times $(t > 1\,\text{ms})$ is shown to be similar for all rupture times tested.

Influence of subgrid-scale model on macro-scale droplet dynamics

To enable a comparison of the present model with previous VOF simulations from the literature that have not used a multi-scale approach (Jiang and James, 2007; Li and Fritsching, 2011), simulations were undertaken *with* (Fig. 8a) and *without* (Fig. 8b) the subgrid-scale model employed. In both cases, a rupture time $t_{rupture}$ of 0.3 ms was imposed for the switching of the ghost-cell boundary condition. For the simulations without the subgrid-scale model, free-slip boundary conditions were used on the collision plane.

The two approaches are shown to give comparable results, indicating that the presence of the subgrid-scale model does not significantly affect the pre-coalescence behavior of the droplets at the macro scale.

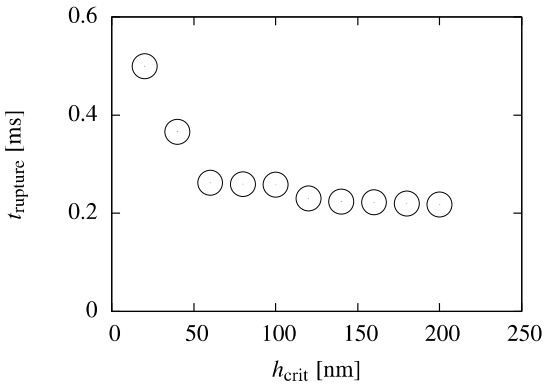

Figure 6: Film rupture time ($t_{rupture}$) dependency on critical film thickness (h_{crit})

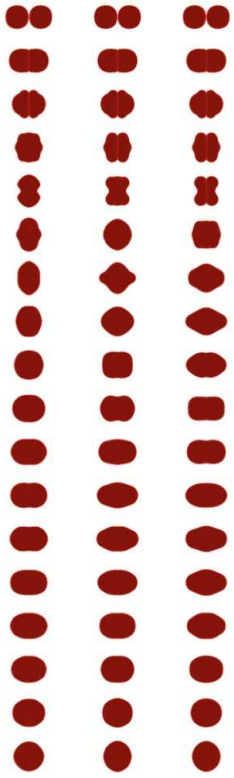

(a) 0.2 ms **(b)** 0.3 ms **(c)** 0.4 ms

Figure 7: Sensitivity to film rupture time (using subgrid-scale gas-film model): (a) $t_{crit} = 0.2$ ms, (b) $t_{crit} = 0.3$ ms, (c) $t_{crit} = 0.4$ ms. Individual sequences shown at 0.1 ms intervals

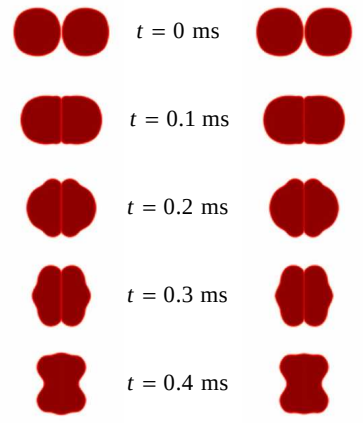

(a) **(b)**

Figure 8: Comparison of droplet evolution (a) *without* subgrid-scale gas-film model and (b) *with* subgrid-scale model. The film rupture time set to 0.3 ms in both cases

Continuum Surface Force accuracy

Surface tension was modelled using the Continuum Surface Force (CSF) model of Brackbill *et al.* (1992). Under the present simulation conditions, in which surface tension is still important ($We \sim 10$), the CSF model is limited by the formation of parasitic velocity currents (Harvie *et al.*, 2006). The magnitude of the parasitic current U_P can be estimated from transient U_T, advection U_A, and viscous U_V terms using the correlation (Harvie *et al.*, 2006):

$$U_P = \min(a_T U_T, a_A U_A, a_V U_V) \tag{11}$$

where:

$$U_T = \frac{2\sigma t_m}{(\rho_g + \rho_l)(W\Delta x)^2} \tag{12}$$

$$U_A = \left(\frac{2\sigma}{(\rho_g + \rho_l) W \Delta x} \right)^{1/2} \tag{13}$$

$$U_V = \frac{2\sigma \max(\rho_g, \rho_l)}{(\rho_g + \rho_l)\min(\mu_g, \mu_l)} \tag{14}$$

Here, a_T, a_A and a_V are code-specific regression constants, Δx is the cell dimension, and t_m is the elapsed simulation time. The non-dimensional interface region width W is defined via $w = W\Delta x$, where w is the dimensional width of the interface region (note that w is defined by the width of the interface region in Eq. (2), which is not the same as the thin-film thickness h). As macro-scale gas dynamics are not calculated in the present code, the limit conditions $\rho_g \to 0$ and $\mu_g \to 0$ can be applied to Eqs. (12)–(14). This gives:

$$U_T = \frac{2\sigma t_m}{\rho_l (W\Delta x)^2} \tag{15}$$

$$U_A = \left(\frac{2\sigma}{\rho_l W \Delta x} \right)^{1/2} \tag{16}$$

$$U_V \to \infty \tag{17}$$

In this case $U_P = \min(a_T U_T, a_A U_A)$, and the velocity errors increase with increasing mesh refinement.

To observe the generation of parasitic velocity currents, a stationary spherical droplet test was undertaken. In an ideal model, the droplet would remain stationary with uniform curvature as the initial velocity of all cells was set to zero and gravitational forces removed.

Stationary droplet test results for the present VOF model show the formation of parasitic currents (Fig. 9). The magnitude of the maximum radial, u_{max}, and axial, v_{max}, velocities increased from zero to of order 1 m/s during a time of 0.4 ms (on the order of the actual collision time scale). Fig. 9 also shows an estimate of the parasitic current using the correlation of Eq. (11). For the mesh resolution used ($\Delta x = 5.0 \times 10^{-6}$ m), the advection term $a_A U_A$ is the controlling term in the correlation. Here, it has been assumed the regression constants of Harvie *et al.* (2006) are directly applicable to the present (different) code.

Parasitic current formation places restrictions on the maximum mesh resolution used in the present simulations, as U_T and U_A, in Eqs. (15) and (16) respectively, both increase with decreasing values of Δx. Additional simulations were undertaken (not shown) that confirmed this prohibitive increase in parasitic current with increasing mesh resolution. The parasitic current terms also increase with increasing surface tension, or (equivalently) decreasing *We*, meaning that the present code cannot accurately predict macro-scale droplet behaviour under low-*We* collisions. The present code is a proof-of-concept model for subgrid-scale coupling. It is envisioned that a more robust model suitable for the entire

range of relevant *We* conditions will be developed using a coupled level-set and VOF (CLSVOF) methodology.

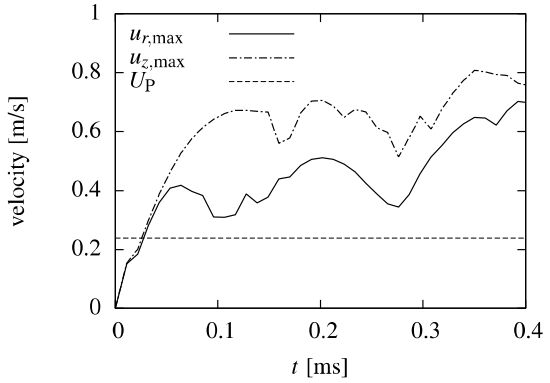

Figure 9: Generation of parasitic velocity currents for a stationary droplet test over a characteristic collision time scale. The maximum radial $(u_{r,\max})$ and axial $(u_{z,\max})$ liquid velocities are shown together with the correlation result of Harvie *et al.* (2006) given by Eq. (11)

CONCLUSION

A coupled VOF and subgrid-scale film drainage model has been used to simulate the symmetric binary collision of tetradecane droplets in air. The film rupture time was found to be sensitive to the value of the critical film thickness used. An experimental collision sequence (Pan *et al.*, 2008) was reproduced using a value of $h_{\text{crit}} = 40$ nm, consistent with experimentally determined values of the critical film thickness (MacKay and Mason, 1963; Bradley and Stow, 1978). The present model demonstrates the applicability of multi-scale modelling techniques to this system, and will be further developed to model industrially relevant coalescence processes.

ACKNOWLEDGEMENTS

Support from the Australian Research Council and the Particulate Fluids Processing Centre is gratefully acknowledged. L. R. Mason acknowledges support from a CSIRO OCE Postgraduate Scholarship

REFERENCES

ASHGRIZ, N. and GIVI, P., (1989), "Coalescence efficiencies of fuel droplets in binary collisions", *Int. Commun. Heat Mass*, **16**, 11-20.

ASHGRIZ, N. and POO, J. Y., (1990), "Coalescence and separation in binary collisions of liquid drops", *J. Fluid Mech.*, **221**, 183-204.

BRACKBILL, J. U., KOTHE, D. B., and ZEMACH, C., (1992), "A continuum method for modeling surface tension", *J. Comput. Phys.*, **100**, 335-354.

BRADLEY, S. G. and STOW, C. D., (1978), "Collisions between liquid drops", *Philos. Trans. R. Soc. Lond.*, **A287**, 1349, 635-675.

CRISTINI, V. and Tan, Y.-C., (2004), "Theory and numerical simulation of droplet dynamics in complex flows – a review", *Lab. Chip.*, **4**, 257-264.

DAVIS, R. H., SCHONBERG, J. A., and RALLISON, J. M., (1989), "The lubrication force between two viscous drops", *Phys. Fluids A: Fluid Dyn.*, **1**, 77-81.

HARDT, S., (2005), "An extended volume-of-fluid method for micro flows with short-range interactions between fluid interfaces", *Phys. Fluids*, **17**, 100601.

HARVIE, D. J. E., (1999), "A hydrodynamic and thermodynamic simulation of droplet impacts on hot surfaces", PhD thesis, Department of Mechanical and Mechatronic Engineering, The University of Sydney, 1999.

HARVIE, D. J. E. and FLETCHER, D. F., (2001), "A hydrodynamic and thermodynamic simulation of droplet impacts on hot surfaces, Part I: theoretical model", *Int. J. Heat Mass Tran.*, **44**, 2633-2642.

HARVIE, D. J. E., DAVIDSON, M. R., and RUDMAN, M., (2006), "An analysis of parasitic current generation in Volume of Fluid simulations", *Appl. Math. Model*, **30**, 1056-1066.

HIRT, C. W. and NICHOLS, B. D., (1981), "Volume of fluid (VOF) method for the dynamics of free boundaries", *J. Comput. Phys.*, **39**, 201-225.

JANSSEN, P. J. A., and ANDERSON, P. D., (2011), "Modeling film drainage and coalescence of drops in a viscous fluid", *Macromol. Mater. Eng.*, **296**, 238-248.

JIA, W. and Qiu, H.-H., (2003), "Experimental investigation of droplet dynamics and heat transfer in spray cooling", *Exp. Therm. Fluid Sci.*, **27**, 829-838.

JIANG, X. and JAMES, A., (2007), "Numerical simulation of the head-on collision of two equal-sized drops with van der Waals forces", *J. Eng. Math.*, **59**, 99-121.

JIANG, Y. J., UMEMURA, A., and LAW, C. K., (1992), "An experimental investigation on the collision behaviour of hydrocarbon droplets", *J. Fluid Mech.*, **234**, 171-190.

LI, X. G. and FRITSCHING, U., (2011), "Numerical investigation of binary droplet collisions in all relevant collision regimes", *J. Comput. Multiphas. Flows*, **3**, 207-224.

MACKAY, G. D. M. and MASON, S. G., (1963), "The gravity approach and coalescence of fluid drops at liquid interfaces", *Can. J. Chem. Eng.*, **41**, 203-212.

MOSTAGHIMI, J., CHANDRA, S., GHAFOURI-AZAR, R., and DOLATABADI, A., (2003), "Modeling thermal spray coating processes: a powerful tool in design and optimization", *Surf. Coat. Tech.*, **163-164**, 1-11.

NIKOLOPOULOS, N., NIKAS, K.-S., and BERGELES, G., (2009), "A numerical investigation of central binary collision of droplets", *Comput. Fluids*, **38**, 1191-1202.

NOBARI, M.R., JAN, Y.-J., and TRYGGVASON, G., (1996), "Head-on collision of drops—A numerical investigation", *Phys. Fluids*, **8**, 29-42.

PAN, K.-L., LAW, C.K., and ZHOU, B., (2008), "Experimental and mechanistic description of merging and bouncing in head-on binary droplet collision", *J. App. Phys.*, **103**, 064901.

QIAN, J. and LAW, C. K., (1997), "Regimes of coalescence and separation in droplet collision", *J. Fluid Mech.*, **331**, 59-80.

RABE, C., MALET, J., and FEUILLEBOIS, F., (2010), "Experimental investigation of water droplet binary collisions and description of outcomes with a symmetric Weber number", *Phys. Fluids*, **22**, 047101.

THOMAS, S., ESMAEELI, A., and TRYGGVASON, G., (2010), "Multiscale computations of thin films in multiphase flows", *Int. J. Multiphas. Flow*, **36**, 71-77.

ZHANG, P. and LAW, C. K., (2011), "An analysis of head-on droplet collision with large deformation in gaseous medium", *Phys. Fluids*, **23**, 042102.

